The effect of chemical species on the electrochemical reactions and corrosion product layer of carbon steel in CO 2 aqueous environment: A review

Edoardo Basilico, Sabrina Marcelin, Remy Mingant, Jean Kittel, Marion Fregonese, Francois Ropital

The effect of chemical species on the electrochemical reactions and corrosion product layer of carbon steel in CO_2-aqueous environment, a review

Contaminants effect on CO_2 corrosion, a review

Edoardo Basilico [1,2*], Sabrina Marcelin [2], Remy Mingant [1], Jean Kittel [1], Marion Fregonese [2], Francois Ropital [1,2]

[1] IFP Energies nouvelles, Rond-point de l'échangeur de Solaize, BP 3, 69360 Solaize, France

[2] Univ. Lyon, INSA-LYON, MATEIS UMR CNRS 5510, 69621 Villeurbanne cedex, France

*Corresponding author Edoardo Basilico IFP Energies nouvelles, Rond-point de l'échangeur de Solaize, BP 3, 69360 Solaize, France. Mail : edoardo.basilico@ifp.fr

Abstract

This paper summarizes the chemical effects that can occur during the corrosion process of carbon steel in a CO_2 saturated aqueous environment. Particularly, it focuses more on the results that small chemical contaminations in the environment have on the corrosion process. Underground waters present complex chemistry with several different dissolved ions (chlorides, carbonates) even in high concentrations that impact substantially on the corrosion rates of these materials. Moreover, gas impurities present in the gas mixture, such as oxygen in carbon capture and storage applications, constitute a supplementary form of significant contamination in the CO_2 saturated aqueous environment.

In particular, the effect on both electrochemical reactions and corrosion product layer is examined for several chemical species that are commonly present either in the gas mixture or in underground waters.

Keywords

CO_2 corrosion, oxygen, carbon-steel, chlorides, contamination.

1 Introduction

Carbon steel remains the most popular material for industrial applications because of its lower cost with respect to corrosion resistant alloys [1][2]. Nevertheless, inferior corrosion resistance performances lead to a deep investigation of the corrosion process in various environments. Furthermore, numerous actions were adopted to prevent corrosion rate value to reach unsustainable costs, such as corrosion inhibitors, cathodic protection and coatings. In relation to a deep knowledge of the corrosion mechanisms, each method of protection has to be designed carefully in order to successfully address the specific corrosion problem.

This bibliographic report concerns the issues related to carbon steel corrosion in a CO_2 water solution, particularly the effects of some chemical elements of the solution that can impact the mechanism of the electrochemical reactions of the corrosion process. Their effects may be direct or indirect through modifications of the nature of the corrosion product layer (CPL).

Understanding and mitigation of CO_2 aqueous corrosion of carbon steels is a major challenge in many industries such as oil production (including enhanced oil recovery EOR), CO_2 capture, transportation, storage and utilization (CCU), biofuels refining and geothermal energy production. Considering the

oilfield brines and oils, their composition is quite complex with a plethora of chemicals that can interact with carbon steel [3] [4]. Therefore a small selection of common water components and those presenting new challenges for carbon capture and storage and geothermal energy production are presented.

Identifying the chemical mechanism that impacts those processes is necessary to plan appropriate interventions for preserving the integrity of the metallic materials. In fact, CO_2 (sweet) corrosion can also be dangerous due to non-uniform scales precipitation, or the formation of less protective corrosion deposits (chukanovite, goethite). As a result pitting-like phenomena and galvanic coupling can also take place leading to unexpected failure of the material [5][6].

Firstly an introduction on the homogeneous chemical reactions that are present in the solution is given, then the effect of CO_2 on both cathodic and anodic reaction is discussed. Cementite, which is a carbon steel phase, impact on the corrosion process intervening in the precipitation of the corrosion product layer and the electrochemical reaction mechanism. This subject constitutes the following part. Finally, the solution contaminants is considered. In particular, most commonly find contaminants such as Ca^{2+}, Cl^- and O_2 are examined.

2 The homogeneous chemical reactions in the CO_2 aqueous environment

The main chemical species present in the CO_2 aqueous environment are carbonic acid and its related ions. Carbonic acid forms in the solution because of the hydration process of dissolved CO_2 [7], which is responsible for complex solution chemistry that determines the aggressiveness of the environment towards the metal. Carbon dioxide dissolution into water is the first step of the process and CO_2 dissolved concentration can be calculated through Henry's Law reported in Equation 1[8]. If not specified all chemical species are intended as dissolved into the solution.

$$[CO_2] = K \cdot p_{CO_2}$$

Equation 1 Henry's law

The *K* constant is dependent on temperature and salt concentration. Afterward dissolved carbon dioxide undergoes a hydration reaction that produces carbonic acid H_2CO_3 (Table 1 a).

Homogeneous solution reaction	Equilibrium constant equation	
$CO_2 \leftrightarrows H_2CO_3$	$K_{Hyd} = \frac{[H_2CO_3]}{[CO_2]}$	a)
$H_2CO_3 \leftrightarrows H^+ + HCO_3^-$	$K_{a1} = \frac{[HCO_3^-]\cdot[H^+]}{[H_2CO_3]}$	b)
$HCO_3^- \leftrightarrows H^+ + CO_3^{2-}$	$K_{a2} = \frac{[CO_3^{2-}]\cdot[H^+]}{[HCO_3^-]}$	c)

Cathodic reactions	
$\mathrm{H^+ + e^- \rightarrow \frac{1}{2}H_2}$	d)
$\mathrm{HCO_3^- + e^- \rightarrow \frac{1}{2}H_2 + CO_3^{2-}}$	e)
$\mathrm{H_2CO_3 + e^- \rightarrow \frac{1}{2}H_2 + HCO_3^-}$	f)
$\mathrm{H_2O + e^- \rightarrow \frac{1}{2}H_2 + OH^-}$	g)

Table 1 Homogeneous and electrochemical reaction table.

In an open system, namely a system where carbon dioxide partial pressure remains constant, the carbonic acid concentration is constant as well. H_2CO_3 is a mild acid with two dissociation constants K_{a1} and K_{a2}, hereafter the reactions involving carbonic acid dissociation are reported along with their respective equilibrium equations ((Table 1 b-c)).

Dissociation reactions are responsible for both a reduction of solution pH, which favors corrosion, and the presence of carbonate ions that are involved in the iron carbonate scales formation [5].

Moreover, under certain conditions, the carbonate ions precipitate with the iron cations Fe^{2+} produced by the anodic electrochemical reaction forming a corrosion product layer that may hinder further metal corrosion as illustrated in **Erreur ! Source du renvoi introuvable.**. In fact, these metallic ions can react with the carbonate ions in the solution in order to give iron carbonate (Reaction 1). It is important to take into consideration the the supersaturation factor (*SS*) that is the product of the

ions concentration forming the precipitate over the solubility constant of the substance (Equation 2)[9]. Precipitation can occur in the case of *SS>1 only*.

$$SS = \frac{[Fe^{2+}][CO_3^{2-}]}{K_{sp}}$$

Equation 2 Supersaturation factor equation

$$\mathrm{Fe^{2+} + CO_3^{2-} \longrightarrow FeCO_{3\,(s)}}$$

Reaction 1 Iron carbonate precipitation reaction.

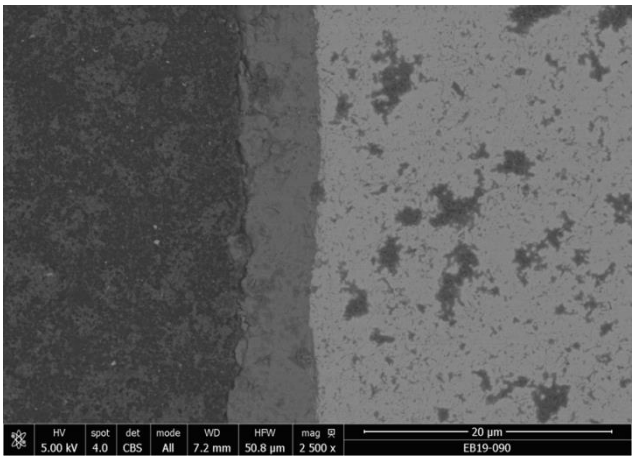

Figure 1 Cross section SEM micrograph of the corrosion product layer of a CO_2 saturate water solutionat 80°C pH 6.8.

Some empirical equations were proposed to model the ion consumption rate due to the scales precipitation. Most of the equations are based on the measure of iron concentration inside the solution throughout the precipitation reaction in static conditions.

The Johnson & Thompson and Greenberg & Thomson equation (**Erreur ! Source du renvoi introuvable.**) were simplified by Van Hunnick *et al.* with the substitution of the iron ion and carbonate activities with their concentrations which are easier to determine (Equation 4) [9] [10].

The expressions of Johnson & Thompson and Greenberg & Thomson Equations are the same but they were obtained with a different experimental method. The main difference consists in the values of the kinetic constant and solubility products present in both equations.

Furthermore, Johnson & Thompson and Greenberg & Thomson equations were verified for low values of supersaturation observing the precipitation starting from seed crystals. In fact the model was developed for bulk precipitation inside a supersaturated solution on seed crystals [10,11]. On the contrary, Van Hunnick formula which was developed using a $FeCO_3$ data bank (**Erreur ! Source du renvoi introuvable.**), can takes into account higher supersaturation values (which are those that occur in the corrosion conditions) [9,10,12].

$$Precipitation\ rate_{FeCO_3} = k_r \frac{A}{V} K_{ps} \left[\left(a_{Fe^{2+}} a_{CO_3^{2-}} \right)^{0.5} - K_{ps}^{0.5} \right]^2$$

Equation 3 Johnson &Thomson equation and Greenberg & Thomson equation where kr is the rate constant Kps is the solubility product, A/V is the ration surface over volume, a represents the activities.

$$Precipitation\ rate_{FeCO_3} = k_r \frac{A}{V} K_{ps}(S-1)(1-S^{-1})$$

Equation 4 Van Hunnick equation, where kr is the rate constant Kps is the solubility product, S is the supersaturation factor, A/V is the ration surface over volume.

Another important parameter in the Van Hunnik formula is the metallic surface (A) over the solution volume (V) ratio. Nesic *et al.* considered this ratio as zero inside the bulk solution and no precipitation would be possible there [13]. Considering that a nucleation step is necessary for the precipitation of any crystal, and the case of siderite precipitation on the active surface, the nucleation is quite fast [14]. Moreover, considering that when the carbon steel is in service, the carbonates precipitate at the metal surface itself and the volume is the one of the fluid in contact with this surface. It could be noted the ratio *A/V* coincides with the degree of confinement, therefore a higher degree of confinement corresponds to a higher precipitation rate. Furthermore, according to the same study, the precipitation rate constant depends on the temperature following an Arrhenius law, which reflects the importance of temperature on the scale precipitation and thus, the protectiveness against corrosion.

However, the iron carbonate nucleation and growth are possible inside the bulk solution as well [15]. Therefore, Sun *et al.* developed a method using mass-loss / mass gain measurements to determine the mass of $FeCO_3$ that precipitated at the surface. Equation 5reports the corrosion layer accumulation rate (CLAR) per unit area. Sun Equation predicts better than Van Hunnick Equation the deposited corrosion product layer mass in low saturation conditions. Moreover, a scaling tendency parameter (Equation 6) was proposed to take into account the undermining effect of corrosion rates of the scales particularly at low supersaturation.

$$CLAR = k_r K_{ps}(S-1)$$

Equation 5 Precipitation equation for CLAR [15].

$$Scaling\ tendency = \frac{CLAR}{Corrosion\ rate}$$

Equation 6 Scaling tendency factor [15].

Aqueous CO_2 corrosion system is rather complex with an interplay of homogeneous-electrochemical and heterogeneous reactions that occur at the same time on the steel surface. These strong bounds between different processes impact greatly the electrochemical reaction and thus the corrosion rates. Finally, from the compresence of iron ions and carbonates, corrosion product precipitation occurs, some equations relating the ion concentration and precipitated mass were proposed but their relation with the corrosion rate has still to be found.

3 The role of carbon dioxide in the electrochemical reactions

Carbon dioxide alters the solution chemistry of the water solution, the concentration of carbonate species depends on the solution pH. The role of carbon species is not limited to the homogeneous chemical reactions but they affect the electrochemical reactions as well. Particularly, both the cathodic and anodic reactions are affected by the presence and concentration of those species. However the mechanism by which those effects take place are still debated both in the anodic and cathodic reaction case. At open circuit potential, anodic and cathodic reaction occurs at the same

place originating a « mixed potential » electrode which is the core of the corrosion process. Understanding the electrochemical reactions involved is important to well understand the corrosion mechanisms of the carbon steel.

The species that participate in the electrochemical reactions are governed by the solution physicochemical parameters such as pH, CO_2partial pressure. Temperature plays a double role affecting both the kinetic of the electrochemical and corrosion product precipitation reactions and the homogeneous reaction equilibria.

3.1 Cathodic reaction

The chemical environment influences greatly the conditions of the cathodic mechanisms in a CO_2 aqueous environment. Temperature as for any other chemical reaction is a key parameter. The pH of the solution determines the aggressiveness towards the metal surface and it affects the precipitation of a corrosion protective layer that can protect the surface.

The literature reports the influence of the carbonate ions on the cathodic reactions following two different approaches: the direct reduction of those ions and the "buffering effect". Those two mechanisms do not exclude each other but understanding which one is more relevant to explain carbon dioxide influence over the corrosion rate is crucial.

The "buffering effect" takes into account only the proton reduction (Reaction 2 a) whereas the direct reduction of carbonic acid and bicarbonate ion is deemed possible in the case of a direct reduction mechanism (Reaction 2 b-c). In the "buffering effect" the contribution of carbonic acid and bicarbonate ion acts simply as a reservoir of protons to be reduced.

a) $H^+ + e^- \rightarrow \frac{1}{2}H_2$ c) $H_2CO_3 + e^- \rightarrow \frac{1}{2}H_2 + HCO_3^-$

b) $HCO_3^- + e^- \rightarrow \frac{1}{2}H_2 + CO_3^{2-}$ d) $H_2O + e^- \rightarrow \frac{1}{2}H_2 + OH^-$

Reaction 2 Cathodic reactions for carbon steel in CO_2 aqueous solution. Only electrochemical reaction a) is considered in the buffering effect mechanism

A rotating disk electrode was used by Remita *et al.* to quantify the contribution of the buffering effect related to the bicarbonate ions [16]. The measured potentiodynamic polarization curves both in CO_2 saturated and deaerated solutions showed a potential zone with a kinetic control regime and, at higher potentials, a mass-transfer control one. The cathodic limiting currents were higher in the presence of carbon dioxide but they did not follow a linear function versus the square root of the electrode rotation speed as per Levich's equation. The authors developed a model considering only the proton reduction and the buffering effect: this model fitted with the experimental polarization curves for each rotation speed and both the desaturated and the CO_2 cases. Therefore, it has been proved the higher limiting current measured for the CO_2 case could be explained without considering acid carbonate or bicarbonate electrochemical reduction. Moreover confronting the two solutions, the cathodic currents in the kinetic control potential range have similar values. If the cathodic

reactions mechanism involves the direct reduction of carbonic acid, the presence of carbon dioxide and related ions will produce a higher current even in the kinetic domain.

A similar approach was used by Nesic *et al.* to generalize the buffering mechanism even in the presence of hydrogen sulfide [17,18]. Their model consider proton reduction as the only cathodic reaction possible and the flux equations integrated the rates of the homogeneous reactions of all the acids and conjugated bases present in the corrosive solution. The proposed model is able to foresee even the second limiting current plateau during the cathodic reaction in the presence of H_2S as well as the above-mentioned potentiodynamic cathodic polarization of a CO_2 saturated solution (Figure 2). Nesic *et al.* concluded that the shape of the curves depend on the solution pH and the pKa of the first and second conjugated bases.

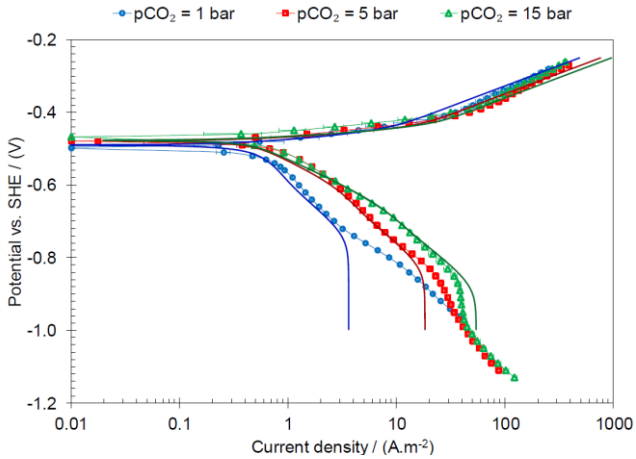

Figure 2 Polarizations curves on API 5L X65 mild steel at 10°C, 0.1 M NaCl, 4.4 m/s flow velocity, at pCO_2 of 1, 5, and 15 bar, at pH 6. Solid lines represent modeling with "buffer mechanism" [18].

On the other side, several authors reported the direct reduction mechanism to explain the higher corrosion rate that was measured in the case of higher carbon dioxide or acetate dissolved concentrations. In another study, Nesic *et al.* reported higher corrosion limiting current in a water solution containing carbon dioxide than in a HCl solution and at the same pH [19]. They attributed this effect to the direct reduction of carbonic acid on the metal surface. However, interpretation is at variance with one of their other studies [20].An increase of the corrosion rate was also observed by Gulbransen *et al.* at increasing the acetic acid concentration in the solution even if the anodic part, *i.e.* iron dissolution, was inhibited as showed by potentiodynamic polarization [21]. This effect on the corrosion rate measured with LPR and mass-loss was attributed to the direct reduction of carbonic and acetic acid.

3.2 Anodic reaction

The anodic reaction (corresponding to the iron dissolution), depends on several factors such as the solution chemistry and the gas contribution. Moreover, the presence of a corrosion deposit may limit the anodic reaction and in doing so the corrosion process [22].

Several solution chemistry parameters contribute to the iron dissolution kinetic. Clearly, temperature as for all chemical reactions plays an important role. Moreover the pH is also essential for the anodic reaction because it changes the concentration and the formation kinetics of the intermediate adsorbed species on the metal surface [23,24]. The presence of other ions in the solution may limit or enhance the general corrosion or more localized forms such as pitting depending on the nature of

the ions and their concentration. The effects can even be indirect, meaning that the presence of some ions can alter through a homogenous reaction, other solution properties such as the pH or the composition, morphology and precipitation kinetics of the corrosion products.

Two possible mechanisms through which the cathodic reactions take place were identified. However the anodic reaction pathways of iron dissolution in the presence of carbon dioxide are still debated because the role of CO_2 is still discussed. In particular, its adsorption on a free metal surface or on any other intermediate specie has not yet been fully elucidated.

$$Fe + FeOH_{ads} \rightleftarrows [Fe(FeOH_{ads})]$$

$$[Fe(FeOH_{ads})] + OH^- \xrightarrow{rds} FeOH^+ + FeOH_{ads} + 2e^-$$

$$FeOH^+ + H^+ \rightleftarrows Fe^{2+} + H_2O$$

Reaction 3 Heusler anodic iron dissolution mechanism [25].

Determination of the anodic reaction mechanism is a key step in order to foresee the kinetic of the corrosion process. Heusler and Bockris investigated the system using steady state techniques proposing two different mechanisms with an anodic slope of 30mV/dec and 40 mV/dec respectively [25–27]. The Heusler mechanism was dubbed catalytic whereas Bockris mechanism was called consecutive. Their reaction pathways are reported in reaction 3 (Heusler) and 4 (Bockris), respectively. However, the only use of steady state techniques has been discussed and considered as not sufficient for unveiling an electrochemical reaction mechanism. Steady-state and transient techniques should be used together in order to have a complete picture of the ongoing electrochemical processes to allow the identification of all the mechanisms and on the presence of intermediates at the surface.

$$Fe + H_2O \rightleftarrows FeOH_{ads} + H^+ + e^-$$

$$FeOH_{ads} \xrightarrow{rds} FeOH^+ + e^-$$

$$FeOH^+ + H^+ \rightleftarrows Fe^{2+} + H_2O$$

Reaction 4 Bockris anodic iron dissolution mechanisms [26,27].

The involvement of carbon dioxide in the anodic process of iron dissolution remains not clear in the literature. A mechanism involving a complex Fe-CO_2 formed through a direct adsorption of carbon dioxide on the metal surface (Reaction5) was proposed by Nesic *et al.* [28]. It was used to explain the different orders of reaction and Tafel slopes measured in different pH and P_{CO2} conditions. Similarly, the role of carbon dioxide on the anodic reactions was investigated by Kahyrian *et al.* through steady state techniques at different CO_2 pressures [29]. The authors claimed that the involvement of CO_2 in the reaction was proved by the slightly different Tafel slopes coefficient for different carbon dioxide partial pressures. Wright *et al.* used potentiodynamic polarization in CO_2 saturated and deaerated solutions [30] for different pH of the electrolyte adjusted using either NaOH or $NaHCO_3$/Na_2CO_3 to have different ions concentration in the solution. The results showed higher anodic currents in the case of CO_2 saturated solutions in the presence of carbonate and bicarbonate ions. The authors proposed the exchange current of the anodic reaction linearly depended on the concentration of CO_2, HCO_3^- and CO_3^{2-}. An increase of their concentration would produce higher anodic currents

during the anodic sweep and as a consequence an increase of the corrosion rates. In any case, no detailed mechanism was proposed in this work. The effect of carbonate ions (CO_3^{2-}) on deaerated and CO_2 saturated aqueous solutions at high pH conditions was studied by Martinelli-Orando *et al.* [31] where two buffer solution, namely HCO_3^-/CO_3^{2-} and borate/NaOH, were tested with a pH equal to 9.8. The potentiodynamic polarization experiments also showed higher currents during the anodic sweep in the case of a CO_2 saturated solution. The authors suggested that the precipitation of iron carbonates lowers the equilibrium potential of the anodic reaction due to a lower concentration of Fe^{2+} ions. They proposed as well a direct reduction of HCO_3^- that led to a rise of the open circuit potential (OCP) and an increase of the corrosion current density (i_{corr}). Therefore the presence of CO_2 and carbonates have opposite outcomes related to the magnitude of i_{corr} but the authors were not able to determine which of the two mechanisms is predominant.

$$Fe_{(s)} + CO_2 \leftrightarrows Fe_L$$

$$Fe_L + H_2O \leftrightarrows Fe_LOH_{(ads)} + H^+ + e^-$$

$$Fe_LOH_{(ads)} \xrightarrow{rds} Fe_LOH^+_{(ads)} + e^-$$

$$Fe_LOH^+_{(ads)} + H_2O \leftrightarrows Fe_L(OH)_{2\,(ads)} + H^+$$

$$Fe_L(OH)_{2\,(ads)} \leftrightarrows Fe_L(OH)_{2\,(sol)}$$

$$Fe_L(OH)_{2\,(sol)} + 2H^+ \leftrightarrows Fe^{2+} + H_2CO_3$$

Reaction 5 Iron dissolution mechanism at pH>5 [28].

Nevertheless, The Tafel slope coefficients obtained in Kahyrian study [32] were not so dissimilar and they could be explained by an experimental error as it was observed by Mattos et *al.* [33]. Moreover, they affirmed the use of steady-state technique only is not sufficient to prove the contribution of carbon dioxide on the iron dissolution reaction. In fact, the importance of supporting the steady state technique results with those obtained through transient techniques such as electrochemical impedance spectroscopy (EIS) was highlighted. Later, EIS was used by Mattos *et al.* to verify the effect of different carbon dioxide partial pressures at pH 4 [34]. They observed one inductive loop attributed to the adsorption of FeOH intermediates as it was previously identified by Keddam [23,24]. Moreover, through an impedance mechanism analysis, the authors showed that at the studied pH, an eventual direct adsorption of CO_2 would produce a second inductive loop. Therefore, Mattos *et al.* concluded that no direct adsorption of carbon dioxide on the metal surface occurred but they did not exclude an eventual adsorption of carbon dioxide on other surface intermediate species. Nevertheless, Mattos *et al.* drawn their conclusion from the above-mentioned impedance measurements performed at pH 4 only: this does not take into account the great variety of environmental conditions that can be encountered dealing with CO_2 corrosion in an aqueous environment.

Similarly to CO_2 adsorption proposed by Nesic *et al.* [28], Hesitao *et al.* explained that sulfur species such as HSO_3^- could adsorb on carbon steel producing higher anodic currents during potentiodynamic polarization in a CO_2/SO_2 aqueous environment. However, even in this study steady-state techniques only were applied [35].

Mattos *et al.* investigate the effect of chloride ions on the carbon steel iron dissolution mechanism [36]. The interpretation of the impedance diagrams proposed that chloride above a critical concentration influences the secondary reaction pathways forming a Fe**(I) oxidized species different from that proposed in the Keddam mechanism presented in Figure . Neither in this case, direct adsorption of chloride ions on the bare surface takes place, therefore, the authors used this example besides the above-mentioned experimental results to exclude the possibility of direct CO_2 adsorption on Fe(0).

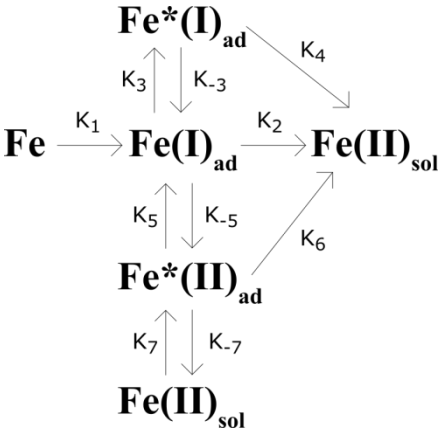

Figure 3 Keddam mechanism schema [23,24].

The carbonic species dissolved into water have a major impact on the electrochemical reactions, the presence of CO_2 increases corrosion rate in the case of two solutions at the same pH either because of direct reduction or "buffering effect" mechanism. An increase of the anodic current was observed with higher carbon dioxide partial pressure. The role of CO_2 in the anodic dissolution has yet to be completely understood. The electrochemical impedance spectroscopy did not allow to observe the direct adsorption of CO_2.

The other actor of the corrosion process is the metal itself, carbon steel plays a minor part if compared to the corrosion of stainless steel, nevertheless the perlite present at the surface plays a role in co-operation with the corrosion product layer.

4 The effect of cementite network on the corrosion in CO_2 aqueous environment.

The corrosion rate of carbon steel in an aqueous CO_2 environment is greatly influenced by the carbon steel microstructure and by the environmental conditions as temperature, CO_2 partial pressure, and the pH. These conditions lead to a formation of a corrosion products layer on the carbon steel surface whose chemical nature plays a role on the corrosion mechanisms. Siderite is the most commonly found phase in the corrosion product layer although other compounds such as chukanovite were reported.

As an example, Fe_3C network that is formed after ferrite dissolution, served as a precipitation network of the iron carbonate corrosion product layer (CPL), increasing the charge transfer resistance of the steel [37]. In fact, electrochemical impedance spectroscopy showed that the precipitation of iron carbonates inside a cementite matrix results in enhanced corrosion resistance due to the physical blocking of the cementite network which is a favorable location of proton reduction.

Kinsella *et al.* also used EIS in order to investigate the properties of the corrosion product layer and the related chemical reactions [38]. The impedance diagrams are characterized by a second time constant at higher frequency when the exposure time increased. Anyway both time constants, have a circular shape on the Nyquist representation for all the pre-scale exposure times. Kinsella *et al.* associated the capacitive high frequency time constant with a protective corrosion product layer, in particular protective scales were formed at higher temperature, pressure and exposure time. No electrochemical mechanism was proposed for the different degrees of protection, nonetheless the higher protection effect was related to smaller crystal size whereas the composition ($FeCO_3$ and Fe_3C) was the same in all conditions.

Pessu *et al.* investigated the effect of temperature on pitting corrosion of carbon steel. Their results in a saturated CO_2 environment at 30°C and atmospheric pressure revealed that in the early stages of the test, both the corrosion rates and OCP were increasing [39,40]. The TEM images (4) showed that ferrite was preferentially dissolved, leaving a rich cementite surface exposed to the corrosive solution. Cementite was proposed to enhance the corrosion rate as it acts as a preferential site for cathodic reduction. Furthermore, the galvanic coupling between the ferrite areas and the nobler Fe_3C produces suitable conditions for pitting. Finally, $FeCO_3$ precipitated in the cementite rich layer, in agreement with Crolet *et al.* work [39].

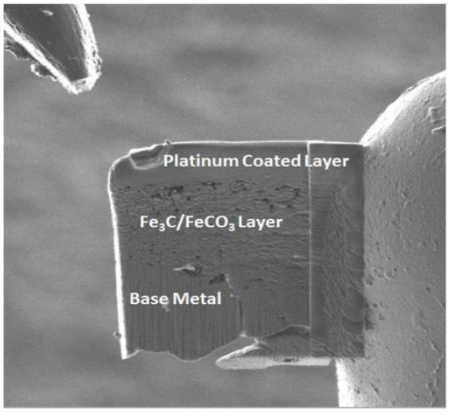

Figure 4 cross section TEM image of a of corrosion product on X65 steel on a CO_2 saturated 10 wt% NaCl at 80°C after 168 h [40].

Moreover, the authors reported that the precipitation of iron carbonate scales could happen on top of the cementite layer. In particular, protective CPLs were only formed when the cementite network was not in contact with the steel surface. For other configurations, the cementite-rich surface could induce a mesa corrosion type attack of the carbon steel. Anyway, an increase in the solution pH was measured in the first stages of corrosion at 30°C, possibly due to the cathodic reduction of H^+. This increase of pH rises the iron carbonate supersaturation, encouraging the $FeCO_3$ precipitation [41]. Later on, the precipitation of the scales protected the surface, stabilizing the corrosion rate value. Acidification of the solution occurs at the ferrite - solution interface, whereas the carbonates precipitation occurs preferentially inside or on top of the cementite matrix. Considering higher temperature conditions, the actual increase of the corrosion rates up to a peak value, was greater than at lower temperatures. Therefore the ferrite selective dissolution and the consequent exposure of a cementite rich surface impacted more the corrosion rates a higher temperature. At 80°C TEM cross-section images confirmed that traces of $FeCO_3$ were present inside the Fe_3C network that can

possibly generate a self-healing mechanism against pits formation. Nonetheless, the cementite effect over the cathodic reactions and its eventual link with pitting corrosion needs further investigations as no specific electrochemical tests have been performed to confirm the electrocatalytic properties of Fe_3C.

5 Influence of contaminants over the corrosion product layer and the corrosion rate

The corrosion product layer that precipitates on the metal surface has a major impact over the corrosion rate. The corrosion product layer is mainly made by iron carbonate, the most common phase found was siderite, although the presence of chukanovite was reported as well [42].

Contaminants in the solution and the gas mix may alter the properties of the corrosion product layer resulting in new form of corrosion such as pitting. Among the numerous chemical species that are dissolved in the complex oilfield waters chlorides and Ca^{2+} alter the CPL morphology resulting in less protective films or pitting corrosion.

Furthermore, oxygen changes the composition of the precipitated products originating several iron oxides. Finally, some experiments revealed the insurgence of pitting corrosion in a CO_2 saturated environment when oxygen was present.

5.1 Corrosion product layers in pure CO_2 saturated water

5.1.1 Corrosion protection of the corrosion product layer

The corrosion product layers (CPL), its morphological structure, or chemical composition have a great influence on the corrosion reactions that occur on the metal surface [42–44]. The formation of the corrosion product layer is strongly interconnected with a variety of factors such as temperature, pH, the composition of the alloy, and of course the chemical species present in the corrosive environment [12,45]. Chemical changes or fluctuations in the environmental conditions result in deviations from the mean protectiveness of the corrosion product layer that may lead to detrimental corrosion morphologies such as pitting.

For example, in the case of carbon steel immersed in a CO_2 aqueous solution, a protective CPL may naturally form at high temperature and pH conditions. The corrosion product layer is formed by iron carbonates that precipitate on the surface when the concentration of Fe^{2+} and carbonate ion is higher than the solubility limit of iron carbonate [46]. Several phases may form at the surface such as $Fe_2(CO_3)(OH)_2$ (Chukanovite) and $FeCO_3$ (Siderite). The latter is more protective of the surface resulting in slower corrosion rates [42].

The mechanism by which the CPL protects the surface is not completely understood. The most probable explanation is that the crystals of the corrosion product layer cover partially the surface diminishing the active surface exposed to the corrosion environment thus decreasing the corrosion rate of the entire surface. Obviously, the coverage of the active surface affects both the cathodic and the anodic reactions slowing them down equally. This results in a constant corrosion potential throughout the exposure to the corrosive environment.

Nevertheless Li *et al.* reported that after a long exposure time, for example at pH 6 and 80°C, the open circuit potential of the corrosion samples raised to higher values [22,47,48]along with a stark decrease of the corrosion rate measured by linear polarization resistance (LPR) (5) [43]. The open-circuit potential rise is not consistent with a simple physical blocking of the surface because it would not have produced any potential shift. The origin of this potential shift and the higher corrosion product layer protectiveness is not clear. In fact, the hypothesis of a reduction of the cathodic reaction rate due to diffusion limitation or pH rise is not supported by the open circuit potential rise which suggests an anodic reaction rate reduction. Other authors agree with the previous analysis in the first period of the corrosion process whereas at longer exposure time, the metal surface is protected by a diffusion limitation of the electroactive species and not simply by the blocking of electrochemically active sites [49].

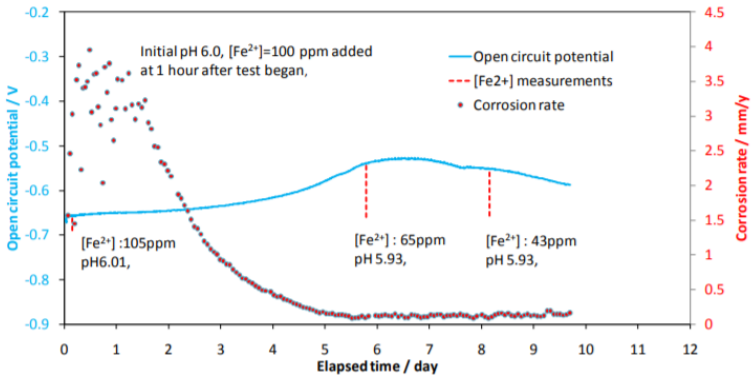

Figure 5 OCP variations and corrosion rate as function of exposure time at 80°C, pH 6.0, 0.53 bar [53 kPa] CO_2, 1 wt% NaCl [48].

5.1.2 Electrochemical considerations about CPL influence over corrosion-rate measurements

The introduction of a diffusion-limited mechanism opens the debate over the correct method for measuring the corrosion rate. Obviously, mass-loss tests are the most reliable in the case of uniform corrosion but they are hard to implement in several industrial applications such as underground pipelines for oil extraction or CCS. Moreover, mass-loss tests can underestimate the danger of more localized corrosion morphologies such as pitting. One of the most diffused methods is to use the LPR in order to measure the polarization resistance which can be converted into the corrosion current using the Stern-Geary relationship [50]. The Stern-Geary relationship is based on the determination of the Stern-Geary coefficient, which can be calculated through the Tafel coefficients of the cathodic and anodic reaction. Unfortunately, the Tafel slopes are not always easily measured because the considered potential range may be too small in some conditions. Finally, the Stern-Geary relationship is based on the assumption that the corrosion is uniform, the electrochemical reactions are mono-electronic, and charge transfer is limited. Therefore, the assumptions that allow using the Stern-Geary relationship are not valid in the case of a diffusion-limited reaction. Nonetheless, for laboratory time scale experiments, LPR techniques may give a good estimation of the corrosion rate since the sample mass-loss is concentrated in the early stages of the test when the assumptions of the Stern-Geary relationship still hold.

5.2 Influence of Chlorides

Chlorides ions have an important impact on the corrosion rate in a carbon dioxide aqueous environment. There is quite a consensus on the effect that chlorides have on the corrosion rate. For an increased content of chlorides, a first increase of corrosion is observed followed by a decrease at higher Cl^- concentrations. Nevertheless, the role of Cl^- on the pitting mechanisms under a corrosion protection layer (CPL) and its breakdown process mechanism, still needs to be further clarified.

The effect of different chlorides concentrations over the CO_2 corrosion of N80 carbon steel was tested by Liu *et al.* [51]. The measured corrosion rates firstly increased up to a maximum with increasing the chlorides concentration and then decreased for higher dissolved chlorides content in the corrosive solution. Furthermore, hand top-view SEM images showed the evolution of the corrosion product layer with increasing chlorides concentration: from a compact layer formed by well-shaped crystals it transformed into bulky, loosely packed crystals that did not effectively cover the carbon steel surface. Additionally, cross-sectional SEM images displayed that the corrosion product layer was formed by an inner compact layer and an outer layer composed of regular crystals. With increasing Cl^- concentration, the boundary between these two layers became less evident and the outer layer crystals had less regular shapes. At the highest tested Cl^- concentrations, *i.e.* 75 g/L, the CPL was thin and barely visible.

Corrosion current obtained from potentiodynamic polarization measurements followed the trend of the mass-loss measurements with a further increase of corrosion current density up to a maximum and then a reduction at higher chlorides content. DRX analysis was in agreement with the results of Ingham *et al.* that found siderite only in the CPL of anodically polarized carbon steel specimens immersed in saturated brine, whereas $Fe_2(OH)_2CO_3$ was present in the same conditions with the addition of $MgCl_2$ [52]. $Fe_2(OH)_2CO_3$ was reported as well by Joshi *et al.* in the first stages of the corrosion process in a CO_2 saturated solution at pH ≈ 4 in the absence of other salts [44].

The corrosion properties and pitting susceptibility of carbon steel was investigated in several corrosive solutions that simulated the sour and sweet operative conditions of Canadian oil pipelines by Papavinasam *et al.* [53]. Electrochemical noise and potentiodynamic polarization techniques were used to investigate this complex system that involved the co-presence of several corrosive gases such as CO_2 and H_2S. Higher values of pitting index and corrosion current densities were found when the chloride concentration was higher. Moreover the authors observed that thinner corrosion product layers were formed at higher chloride concentration and thus they attributed a higher risk of pitting corrosion for greater dissolved Cl^- concentration.

Fang *et al.* investigated the effect of flow and the increase of chlorides concentration in a carbon dioxide saturated water solution on the corrosion of carbon steel [54]. The results showed a diminution of the uniform corrosion rate with increasing NaCl concentration (which is an unexpected result) whereas the corrosion rate increased with a higher rotation of the electrode. Nevertheless, the effect of flow conditions became less important for higher chlorides concentrations. The potentiodynamic polarization indicated that the dissolved NaCl slowed down both the anodic and the cathodic reactions and this behavior was attributed to the change from a mixed charge transfer/limiting current control to a charge transfer control. Finally, no pitting was observed on the metal surface in any of the tested conditions.

A double electrochemical role is attributed to Cl^-: it interacts directly with the iron surface accelerating the anodic reaction while it lowers the CO_2 solubility leading to a decrease of the cathodic reduction rates [55]. Nonetheless, the conclusion related to the anodic reaction is not supported by transient techniques, as the use of steady-state techniques is not sufficient to ascertain a reaction mechanism. The lack of corrosion product precipitation at higher chlorides concentration was attributed to the accumulation of oxygen vacancies at the metal/film interface that stops the growth of the CPL while its dissolution still occurs at the solution/film interface.

Eliyian *et al.* pointed out that the experimental conditions of Papavinasam *et al* [53] and Fang *et al.* [54] namely complex corrosive solution chemistry and the gap between chlorides concentration tested respectively [56] were not ideal in order to isolate the chlorides contribution on the corrosion process . Their potentiodynamic polarizations at progressive chlorides concentration showed a monotonous decrease of corrosion potential whereas the corrosion current increased up to a peak at lower chlorides concentrations and then it platooned at lower corrosion rates for greater concentration values. Those results were obtained for both tested temperatures namely 20°C and 80°C. The authors claim that the corrosion rate declined after the peak value is due to a slower kinetics of the cathodic reactions. In fact, the limiting current plateau during the cathodic polarizations was lower in the high [Cl^-] case. Electrochemical impedance results showed that Cl^- did not impact the overall corrosion process mechanism as the shape of the impedance diagrams on Nyquist plot did not change. Furthermore, impedance measurements performed at high cathodic overpotential displayed that the chlorides do not interfere with the cathodic reduction of protons. Therefore, the slower cathodic kinetics have to be linked to other chemico-physical interactions between the Cl^- ions and the corrosive environment.

CO_2 corrosion of carbon steel at different chlorides concentrations was tested and blank tests were made with Cl^- ions only without CO_2 [57]. The mass loss measurements showed a rise in the corrosion rate for increasing chlorides concentration up to threshold concentration upon which the corrosion rate started to decrease. The impedance measurements did not show variations between the chlorides solutions and the electrochemically inert perchlorate ion. Therefore, Cl^- did not impact the electrochemical mechanism of the corrosion process. This last result is in contrast with the anodic iron dissolution mechanism proposed by Liu *et al.* that involved a direct interaction between the steel surface and Cl^- ion leading to an adsorbed hydroxyl-chloride anion [51]. Moreover, according to these authors, a competitive adsorption occurs between Cl^- and HCO_3^- [58].

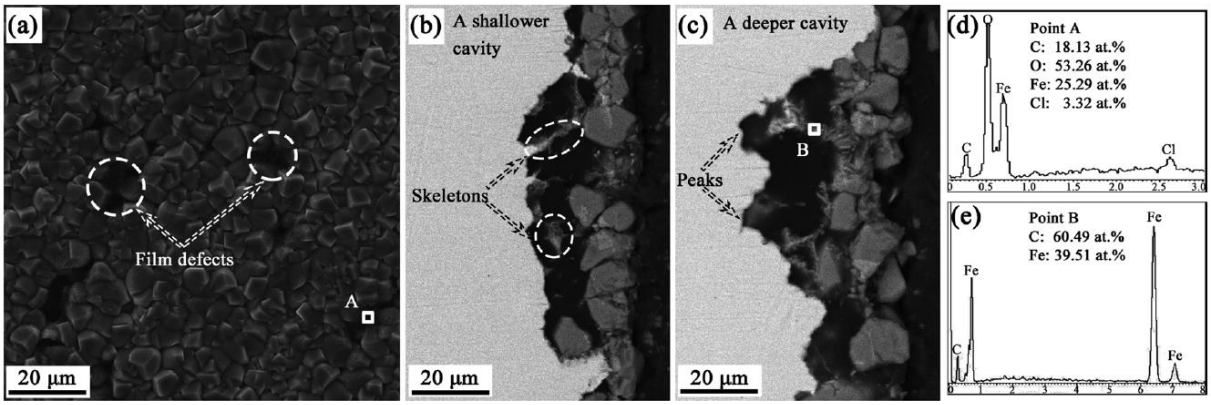

Figure 6 SEM micrographs (a) – (c) of morphologies of corrosion product layer for carbon steel in Cl^- containing CO_2 saturated solution. (d) – (e) relative EDS analysis [57].

However, an injection of chlorides ions resulted in a reduction of the corrosion scales surface coverage. In fact, considering the surface coverage variation at different chloride concentrations, the trend is the opposite of the corrosion rate whereas the crystal size follows the same tendency of corrosion rate. Cross-sectional SEM observations showed that the corrosion product layer is more porous in the presence of chlorides ions, highlighting the formation of less protective scales. Top-view SEM micrographs revealed an increasing number of CPL defects when increasing the Cl^- concentration (Figure 6 [63]). Furthermore, the EDS investigation of the corrosion products in the surroundings of the film defects detected traces of chlorides pointing out the possible involvement of Cl^- in the formation of the film defects. Profilometry measurements of the metal surface after the removal of the corrosion product layer showed more corrosion pits in the solutions containing chlorides than in that simply saturated with carbon dioxide. The authors [63] claimed that the intervention of the chloride ions on the corrosion product layer is related to the decrease of the carbon dioxide solubility inside the solution. This decrease in the carbon dioxide concentration would result in a slower iron carbonate formation because it does not react with $Fe(OH)_2$ thus leading to a less effective diffusion barrier and protection when chlorides are dissolved in the solution. This results in the localization of the anodic areas over the metal surface that initiates pitting corrosion.

A final proposed mechanism involves oxygen vacancies that are promoted by a higher chlorine activity. Accumulation of those vacancies at the interface between the corrosion product film and the metallic surface leads to localized film breakdowns and thus pits formation. This mechanism was also proposed by Liu *et al.* to explain the corrosion product layer breakdown at increasing Cl^- concentration [51].

5.3 Influence of Ca^{2+}

Iron carbonate is not the only precipitate that can be formed at the metal surface. Joshi *et al.* observed the co-precipitation of siderite and chukanovite that is a hydroxicarbonate. The presence of iron oxides was reported below the siderite scales [43,55]. Nonetheless, carbonate anions form many insoluble compounds in the presence of other cations such as Ca^{2+}. In fact calcium carbonate is an isostructural form of the siderite that can readily incorporate Ca^{2+} ions [59] in its structure. Similarly, Fe^{2+} ions can be incorporated into the crystal structure of calcium carbonate. An average calcium concentration ranges between 2.5 and 26 g/L in oilfield waters [60].

Alsaiari *et al.* investigated the interaction between the Fe^{2+} and the calcium carbonate precipitation in a batch reactor [61]. The results showed that Ca^{2+} enhances the siderite ($FeCO_3$) solubility whereas Fe^{2+} does not affect the calcium carbonate solubility. Moreover, the presence of Ca^{2+} attenuated the temperature effect over $FeCO_3$ precipitation *i.e.* siderite precipitated more slowly at 65°C when Ca^{2+} ions were inside the solution. Finally, four precipitation interactions between $CaCO_3$ and $FeCO_3$ were identified. Particularly, one of them displayed the inhibition of the $FeCO_3$ (siderite) nucleation and growth at the beginning of the $CaCO_3$ (aragonite) precipitation. In a later study, calcium carbonate precipitation was found faster than the iron carbonate one despite a higher calcium carbonate solubility. Moreover, higher calcium to iron ratio in the solid than in the solution was found [62]. Finally, the formation of a mixed iron-calcium carbonate $Fe_xCa_{(1-x)}CO_3$ was reported and a method to predict the calcium content in the mixed precipitate using as inputs the concentration values of Ca^{2+} and Fe^{2+} in the solution was developed [63].

Later, the impact of calcium ions on the precipitation of iron carbonates that form the corrosion product layer on the metal surface was highlighted [64]. The corrosion tests showed that for low Ca^{2+} concentration such as 10 and 100 ppm the measured corrosion rate was similar to that of the blank solution whereas, for higher Ca^{2+} concentration (10^3 and 10^4 ppm Ca^{2+}), the corrosion rate was higher. Moreover, the corrosion rate for the lower concentration decreased with exposure time while it remained constant for 10^3 and 10^4 ppm. The presence of calcium ion at higher concentrations corresponded to a lower pH of the solution. According to the authors, the pH shift towards lower values was due to the precipitation reaction of calcium carbonate that produces free H^+. As reported in reaction 2, a pH change can have a dramatic impact on the homogeneous reactions equilibria and saturation values of the corrosion products leading to different outcomes for the CPL protectiveness.

The measurements of the dissolved Fe^{2+} and Ca^{2+} ions in correlation with the related carbonate saturation showed that, after the initial precipitation of iron and calcium carbonates, the iron carbonate precipitation rate became slower due to the lack of available Fe^{2+}. Iron carbonate precipitated at the surface although its saturation rate was significantly lower than the one of calcium carbonate, pointing out a faster kinetic for the $FeCO_3$ precipitation [64]. The minimum value of the $FeCO_3$ saturation was followed by an increase due to corrosion producing free Fe^{2+} ions in the solution leading to a new growth of the iron carbonate saturation rate.

Finally, XRD analysis showed that a mixed iron-calcium carbonate was formed in the higher dissolved Ca^{2+} concentration in association with higher corrosion rates underlining that $CaCO_3$ and the mixed carbonate are less protective than $FeCO_3$. The molar fraction of calcium is not equal along the CPL cross-section but, for the higher values of dissolved Ca^{2+}, it is richer in calcium close to the surface. For lower calcium concentration both the XRD analysis and the SEM top-view images confirmed that dissolved Ca^{2+} did not affect the morphology and crystallographic structure of the corrosion product layer. The increase of calcium molar fraction in the CPL for higher dissolved Ca^{2+} concentration is in agreement with the results of Ding *et al.* that measured the molar fraction of the mixed iron-calcium carbonate using XRD analysis. The results confirmed the presence of calcium ion in the solution made the corrosion product layer less protective [65].

The effect of the calcium ions on the protectiveness in the corrosion product layer was also investigated [66]. Different flow conditions were tested keeping the same concentration of 10^4 ppm of calcium ions. The corrosion rate in the presence of dissolved Ca^{2+} was lower even in flow conditions, contrarily to what was found in the previously mentioned studies. Moreover, as a result of the precipitation of iron carbonate, the solution pH was stabilized to a higher value than without Ca^{2+}. SEM micrographs displayed morphologies that are different from the siderite crystals: probably the CPL should be a mixed iron-calcium carbonate film. Through the analysis of the XRD diffraction {104} inter planar d spacing, a calculation method for the Ca^{2+} fraction of a mixed iron-calcium carbonate was developed.

Moreover, pitting corrosion occurred during the test in stagnant and 300 rpm conditions in the presence of Ca^{2+}. Nonetheless, it was not possible to determine if the above-mentioned pits were filled by the corrosion products and thus stopped or kept propagating. The authors claim that Ca^{2+} ions are responsible for pits formations rather than the Cl^- ion, because they did not observe any pits in the NaCl only solutions whereas they did when Ca^{2+} ions were added. However, the range of

experimental conditions such as temperature and concentration of Cl^- and Ca^{2+} ions is not wide enough to exclude the role of Cl^- in pit formation for iron carbonate scales.

The scales formation in simulated produced water (SPW) was investigated at supercritical CO_2 pressure on carbon steel [67] . Since the corrosive solution used is an oil well simulated produced water (SPW) , dissolved Ca^{2+} is guaranteed by the dissolution of $CaCl_2$. The presence of both Cl^- and Ca^{2+} makes it hard to distinguish the role of each single chemical species on the pitting initiation and propagation or overall pitting risk of the CPL in comparison with a pure saturated CO_2 water solution. Anyway, XPS and XRD analysis confirmed the presence of an iron-calcium carbonate $Fe_xCa_{(1-x)}CO_3$, which was the main phase of the scales, and α-FeOOH was also detected. The composition of the corrosion product layer was in agreement with the observations of Wu et al. that performed corrosion tests with the same solution at a lower pressure (0.5 MPa) [68].

The influence of calcium ion under supercritical CO_2 pressures in aqueous phase was also investigated [69]. In order to provide the desired calcium contamination, an appropriate quantity of solid $CaCO_3$ was added to the autoclave. In supercritical conditions and for all the tested exposure times, the addition of $CaCO_3$ resulted in a lower corrosion rate. For both the blank and the $CaCO_3$ solutions, the corrosion rate decreased over time because of the precipitation of a corrosion prouct layer. Diffusion barrier properties were attributed to the precipitated film, even if SEM observations revealed that the scales that precipitated with the addition of calcium carbonate in the solution were thinner and more porous. Combined XRD and EDS analysis revealed that in the presence of $CaCO_3$ the corrosion product layer is a mixed calcium-iron-carbonate layer. Some precipitation reactions were proposed involving co-precipitation of iron with Ca^{2+} and carbonate-bicarbonate ion or iron with calcium bicarbonate. Finally, the scaled samples were tested using electrochemical measurements as well. The potentiodynamic polarization revealed a passive both with and without $CaCO_3$ but in the latter cases, pits were observed once the “trans-passive” potential was overcome.

Shamsa *et al.* investigated the impact of Ca^{2+} ions over the precipitation of the corrosion product layer and the corrosion protective properties of the film [70]. Experiments were performed in an autoclave at 80°C and 150°C. Two corrosive solutions were tested with and without dissolved Ca^{2+}. The samples were analyzed after different exposure times in order to follow the evolution of the corrosion scales during testing. The corrosion product scales formed at higher temperatures provided superior protection from corrosion although the porosity of the layers was comparable for both temperatures. Moreover, the precipitation of the scales at 150°C occurred during the first 6 hours of exposition in the corrosive environment. Considering the corrosive solution with dissolved Ca^{2+} at 80°C, the scales formed were less protective after four days of testing although the mass of the corrosion film was higher. The precipitation of the CPL in the first 48 hours of the experiment was faster without Ca^{2+}. The relationship between the mass loss and the corrosion product mass after two days showed that the corrosion film was less adherent at the metal surface with the addition of Ca^{2+} ions in the solution due to greater solubility of Fe^{2+} with Ca^{2+} contamination as previously reported by Alsaiari *et al.* [61]. At 150°C the addition of dissolved Ca^{2+} ion resulted in similar corrosion rates than in the NaCl-only solution after four days of exposure to the corrosive environment. However, this similar protectiveness of the deposit was attained with a smaller corrosion film mass. The higher protectiveness obtained at higher temperature is also observed in the profilometry analysis for the investigation of the localized corrosion beneath the CPL. The results show that at 150°C the uniform corrosion rate reaches low values with and without Ca^{2+} in the

solution and that the pit growth is constant throughout the test. On the contrary, at 80°C a higher uniform corrosion penetration was observed for the case with Ca^{2+} ions whereas the pit penetration depth is similar for the two conditions. Therefore the authors claim that Ca^{2+} ions at lower temperatures expose the surface to a higher risk of pitting corrosion as the higher rate of uniform corrosion makes the pit penetration to be underestimated. Higher temperature conditions present the same risk of pitting corrosion regardless of the presence of the Ca^{2+} ions, but the protective scales formed seem to prevent the pitting propagation.

SEM micrographs of the corrosion product layer formed at 80°C after 96 hours of exposure, showed that the film was more porous with the addition of Ca^{2+}. The CPL was formed by a mixture of $FeCO_3$ and iron-calcium carbonate ($Fe_xCa_yCO_3$) that co-precipitated together on top of the metal surface whereas at higher temperature, after the same exposure time, this mixed-phase was embedded inside the $FeCO_3$ film. XRD analysis allowed to determine the evolution of the content of Ca^{2+} ions inside the corrosion product layer. The results showed that the calcium fraction inside the film decreases over time at 80°C, whereas the film precipitated at 150°C had a constant concentration of calcium throughout the all test duration.

5.4 Effect of oxygen

Few studies have reported the effect of oxygen in a CO_2 corroding system. Xiang *et al.* investigated the effect of a complex $CO_2/SO_2/O_2/H_2O$ mixture in supercritical conditions, on the corrosion of X70 carbon steel [71]. In this case, oxygen was considered as an oxidant for sulfites leading to the formation of hydrated sulfates inside the corrosion product film.

Some tests were performed in water-saturated supercritical CO_2 conditions with the addition of traces of oxygen (2000 ppmv), hydrogen sulfide (2000 ppmv) and both the contaminants at the same time [72]. The results showed similar and low values of the corrosion rates for pure CO_2 and mixed CO_2-O_2 system. One order of magnitude higher values were obtained for the CO_2-H_2S system whereas when all the contaminants were present at the same time, a hundred time greater corrosion rate values were observed. Observation of the samples after removal of the corrosion product layer was performed. In the pure CO_2 with oxygen trace cases in supercritical conditions, localized corrosion was observed whereas the other experiments with oxygen and hydrogen sulfide contaminations, displayed a generalized uniform corrosion. Concerning the corrosion product layer, a thin grey film was present with CO_2 and with H_2S contamination. A layer of rust was present when adding oxygen. In the last situation, *i.e.* CO_2-H_2S-O_2, the macroscopic film was present with a loose outer part and an inner more dense layer as shown in 7. This structure of the CPL points out an evolution of the corrosion product film precipitation that cannot be elucidated observing one sample only at the end of the test. SEM images with EDS analysis revealed that small amounts of corrosion products precipitated with CO_2 only, whereas in the case of O_2 worm-like structures were present and they were attributed to Fe_2O_3 because of the iron/oxygen ratio. XRD analysis showed a complex chemistry for the precipitates when all the gases were present. A variety of corrosion products such as $FeCO_3$, S_8, FeS, FeOOH and Fe_2O_3 was identified. As EDS analysis did only show oxides on the surface, the authors proposed that oxygen inhibits the iron carbonate precipitation. The corrosion product layer precipitation was therefore attributed to the iron oxidation products Fe_2O_3 and FeOOH.

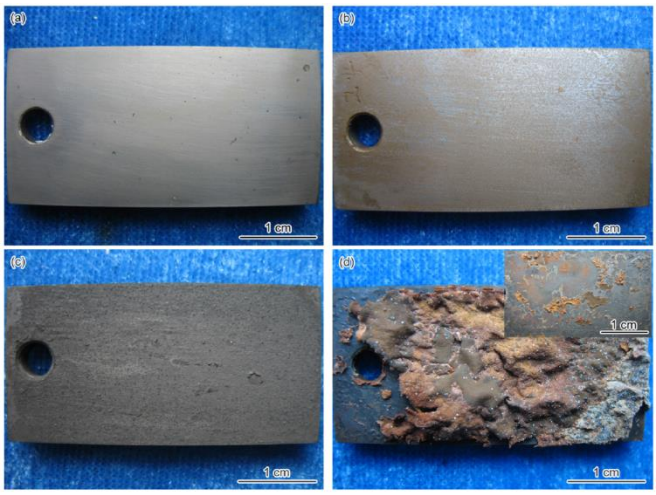

Figure 7 Photograps of corrosion product layer developed at 50°C CO_2, 10 MPa, O_2: 2000 ppmv, H_2S: 2000 ppmv. (a) CO_2; (b) CO_2+ O_2; (c) CO_2+ H_2S and (d) CO_2+ O_2+ H_2S [77].

In another study the effect of oxygen on mild steel samples was investigated [73]. The potentiodynamic polarization results showed that the cathodic reactions of the corrosion process is dominated by charge transfer with oxygen concentration inferior to 100 ppb whereas for higher O_2 concentrations (1 ppm) the mechanism is a mixed control one. Moreover, at 3 ppm after 24 hours, pitting initiation occurred but propagation did not take place. The pits came from the ferric oxide layer that precipitated on the steel surface. Its thickness depended on the oxygen concentration and finally no iron carbonate precipitation occurred due to the low pH value (5) at which the test was carried out.

Oxygen effect on sweet corrosion in enhanced oil recovery situations [74] was studied by Rosli et al. They investigated the impact that the addition of 1 ppm of dissolved oxygen has on carbon steel. The oxygen contamination was added at different exposure times in a water solution at 80°C and pH 6.6. The results revealed that, with the introduction of oxygen, the OCP increased by 200 mV after 48 hours. Furthermore, the corrosion rates measured with O_2 were slightly higher than without oxygen. The corrosion product layer displayed some clusters, mounds and craters that are considered as the porous corrosion products on top of a pit whose outer layer was composed of iron oxides. XRD analysis reflected the SEM observation, identifying hematite and magnetite inside the CPL. The addition of oxygen from the start of the test, resulted in postponing the formation of a protective corrosion product layer as reflected by the measured corrosion rates and the concomitant OCP rise. In the CPL, iron oxides hindered the coverage of $FeCO_3$ because of competitive precipitation.

The effect of oxygen contamination on the composition of carbonates corrosion product layer through in a situ XRD work was studied [75]. The experimental setup consisted of a classical three electrodes electrochemical cell with an API J55 carbon steel as the working electrode. The electrolyte was a 0.5 mol/kg NaCl CO_2 saturated solution. 20g/kg of 2 mol/kg NaOH solution was added to give a calculated pH of 6.8. The operating temperature was set to 80°C as other tests previously discussed for the sake of optimal scaling conditions. Oxygen was not directly introduced into the electrolyte but it diffused through the tubes silicone rubber-made that connected the electrochemical cell with the solution reservoir. Therefore, the oxygen concentration was a function of the solution flow rate into the tubes. In any case, there was no monitoring of the dissolved oxygen concentration, which does not guarantee constant chemical conditions throughout the test.

The working electrode was polarized at different anodic potentials to accelerate the corrosion products layer formation. Furthermore, the oxygen concentration into the cell was changed by regulation of the solution flow thanks to a peristaltic pump. The more the solution flux the less the oxygen was dissolved into the electrolyte.

Although anodic polarization of the working electrode speeds up scaling, it may have influenced the kinetics and thermodynamic conditions of the precipitated compounds.

The addition of oxygen caused the crystallization of green rust immediately after the polarization potential was applied. Green rust composition was identified as $Fe_6(OH)_{12}CO_3$. Unlike the aforementioned mechanism suggested by Ingham where amorphous iron carbonate had first precipitated and then precipitation of crystallized siderite occurred. Crystalline $Fe_6(OH)_{12}CO_3$ appeared also in the first stages *i.e.* dissolution phase of the corrosion process [76].

The volume of the green rust that precipitated was dependent only on the solution flow, *i.e.* the oxygen concentration, and not on the applied anodic potential. However, this phase did not cause a diminution of the current peak value recorded whereas a current fall was observed when siderite crystals were formed on the metal surface. The chukanovite precipitation rate and amount were dependent both of the flow rate and the electrode potential; particularly its amount grew at a lower flow rate, *i.e.* higher oxygen concentration, and its rate had higher values for a more negative electrode potential. However, chukanovite precipitation was faster, with respect to siderite, for higher flow rates at the same potentials. The accelerated precipitation advanced the chukanovite appearance before the siderite one. Because the $Fe_6(OH)_{12}CO_3$ kinetic was only dependent on O_2 concentration and did not correlate with the dissolution current peak, its formation as a direct dissolution product of iron was discarded, therefore the green rust has no direct effect on the precipitation of other iron carbonates. Nonetheless, its formation was explained by oxidation of dissolved iron (II) present in the solution. Oxygen did not affect the siderite precipitation.

Regarding the chukanovite precipitation, the green rust had an indirect effect by altering the surface pH. In fact, the reaction that leads to $Fe_6(OH)_{12}CO_3$ produces almost twice H^+ compared to the siderite precipitation reaction. $Fe_6(OH)_{12}CO_3$ formation was accelerated at a low flow rate, so is the precipitation rate of chukanovite with respect to siderite. However, chukanovite precipitation was faster at lower applied anodic potential when Fe^{2+} supersaturation is lower. The green rust precipitation was unaffected by the applied potential. Therefore at low dissolved iron conditions, the $Fe_6(OH)_{12}CO_3$ precipitation overcomes the siderite one, leading to a decrease in the surface pH that favors chukanovite precipitation over siderite. The formation of secondary phases such as magnetite and FeOOH is attributed to chukanovite further oxidation [77]. In any case nor corrosion rate or weight loss measurements were performed therefore it was not possible to determine which phase is the most protective. Considering the work of Joshi *et al.*, a reasonable assumption would be that siderite is the most effective component that protects the metal surface.

6 Conclusions

Several contaminants affect directly and indirectly the chemical and electrochemical reactions of the corrosion process in the CO_2 aqueous environments, this review aimed to underline the consequences of the presence of the most common contaminants in the corrosive environment.

The main produced effects involve contaminants interaction with the corrosion product layer that indirectly affect the corrosion rates, the corrosion products composition and morphologies formed on a carbon steel surface. The most important aspects of each chemical interaction are hereby summarized:

- Several studies concern the effect of carbonic acid and its related compounds on the corrosion rates in CO_2 environment. These works concentrated mainly on the cathodic reactions debating whether the carbonic acid and its ions are directly reduced at the steel surface or act as an additional source of protons. The CO_2 dissolved concentration has an influence over the iron dissolution mechanism although the exact reaction path is still unknown.

- A cementite layer forms naturally as a consequence of ferrite dissolution on the carbon steel surface in CO_2 aqueous solution. The Fe_3C network offers a mesh where iron carbonate can precipitate. Nevertheless, a low overpotential for H^+ reduction is attributed to the cementite. This assumption needs confirmation with appropriate testing taking into account the origin of the galvanic coupling effect and the local pH variation at the metal surface.

- Ca^{2+} is commonly found in oilfield brines and as Fe^{2+} form an insoluble calcium carbonate precipitate with CO_3^{2-}. In the presence of Ca^{2+} a mixed iron-carbonate phase is formed that can be as much protective as iron carbonate depending on the precipitation conditions. Therefore more specific studies are to be made to understand how this mixed carbonate precipitate at the surface under a wider range of conditions and its impact on the corrosion rate of the reactions.

- Chlorides are one of the most common components in mineral aqueous solution and their effects on the corrosion process are essential. Recent studies clarify the effect of chlorides over the possible corrosion morphologies of carbon steels, in particular by promoting pitting corrosion. A mechanism that still has to be confirmed, was proposed for the corrosion film breakdown.

- Oxygen represents one of the challenges for carbon capture and storage. Besides of its oxidizing power that can interact with specific cathodic sites, its presence can affect the composition of the corrosion product layer introducing significant amounts of different oxides, originating less protective films and pits formation. Studying oxygen introduction in traces at different exposure times and conditions, in order to simulate an industrial contamination, would help to better elucidate the impact that such contamination can have on corrosion in CO_2 aqueous environment.

7 References

[1] D. Dwivedi, K. Lepková, T. Becker, *RSC Adv.* **2017**, *7*, 4580–4610.

[2] T. E. Perez, *JOM* **2013**, *65*, 1033–1042.

[3] T. Boschetti, S. M. Awadh, H. S. Al-Mimar, P. Iacumin, L. Toscani, E. Selmo, Z. M. Yaseen, *Marine and Petroleum Geology* **2020**, *122*, 104637.

[4] B. Bazin, É. Brosse, F. Sommer, *Marine and Petroleum Geology* **1997**, *14*, 481–495.

[5] R. A. de Motte, R. Barker, D. Burkle, S. M. Vargas, A. Neville, *Materials Chemistry and Physics* **2018**, *216*, 102–111.

[6] J. Han, B. N. Brown, and S. Nešić, *CORROSION* **2010**, *66* (9): 095003–095003-12..

[7] a) B. R. Linter, G. T. Burstein, *Corrosion Science* **1999**, *41*, 117–139; b) R. F. Weiss, *Marine Chemistry* **1974**, *2*, 203–215;

[8] a) Z. Duan, R. Sun, C. Zhu, I.-M. Chou, *Marine Chemistry* **2006**, *98*, 131–139; b) Z. Duan, R. Sun, *Chemical Geology* **2003**, *193*, 257–271;

[9] E. van Hunnik, E. Hendriksen, B. F. Pots in , NACE International,paper n° 6, **1996**.

[10] M. L. Johnson, M. B. Tomson, *M. L. Johnson, M. B. Tomson, CORROSION 91/268, NACE, Houston,* **1991**.

[11] J. L. GREENBERG, *High temperature kinetics of precipitation and dissolution of ferrous-carbonate,* MSc Thesis*,* **1987**.

[12] M. Nordsveen, S. Nesic, R. Nyborg, A. Stangeland, *CORROSION* **2003**, *59*, 443–456.

[13] S. Nesic, K.-L. J. Lee, V. Ruzic, *CORROSION/2002, paper* **2002**, *2237*.

[14] S. Nesic, *Energy Fuels* **2012**, *26*, 4098–4111.

[15] W. Sun and S. Nesic, *Corrosion* **2008,** 64 (4): 334–346.

[16] E. Remita, B. Tribollet, E. Sutter, V. Vivier, F. Ropital, J. Kittel, *Corrosion Science* **2008**, *50*, 1433–1440.

[17] a) A. Kahyarian, B. Brown, S. Nešić, *CORROSION* **2020**, *76*, 268–278; b) A. Kahyarian, S. Nesic, *Corrosion Science* **2020**, 108719;

[18] A. Kahyarian,PhD Thesis, Ohio University, **2018**.

[19] S. Nesic, J. Postlethwaite, and S. Olsen *CORROSION* (1996) 52 (4): 280–294.

[20] A. Kahyarian, B. Brown, S. Nešić, *CORROSION* **2018**, *74*, 851–859.

[21] E. Gulbrandsen, K.Bilkova in *CORROSION/2006, Paper no. 06364, NACE*, **2006**.

[22] W. Li, B. Brown, D. Young, S. Nesic in *CORROSION* (2014) 70 (3): 294–302. **2014**.

[23] M. Keddam, O. R. Mattos, H. Takenouti, *J. Electrochem. Soc.* **1981**, *128*, 266.

[24] M. Keddam, O. R. Mattos, H. Takenouti, *J. Electrochem. Soc.* **1981**, *128*, 257.

[25] K. Heusler, *Zeitschrif fur elektrochemie*, **1958,** 62 (5) 582-587.

[26] J. Bockris, D. Drazic, A. R. Despic, *Electrochimica Acta* **1961**, *4*, 325–361.

[27] J. Bockris, D. Drazic, *Electrochimica Acta* **1962**, *7*, 293–313.

[28] S. Nesic, N. Thevenot, J. L. Crolet, D. M. Drazic in Corrosion/96 paper n°3, pp.24-29, **1996**.

[29] A. Kahyarian, B. Brown, S. Nesic, *Corrosion Science* **2017**, *129*, 146–151.

[30] R. F. Wright, E. R. Brand, M. Ziomek-Moroz, J. H. Tylczak, P. R. Ohodnicki, *Electrochimica Acta* **2018**, *290*, 626–638.

[31] F. Martinelli-Orlando, W. Shi, U. Angst, *J. Electrochem. Soc.* **2020**, *167*, 61503.

[32] A. Kahyarian, B. Brown, S. Nesic, *Corrosion Science* **2017**, *129*, 146–151.

[33] T. C. Almeida, M. Bandeira, R. M. Moreira, O. R. Mattos, *Corrosion Science* **2018**, *133*, 417–422.

[34] T. das Chagas Almeida, M. C. E. Bandeira, R. M. Moreira, O. R. Mattos, *Corrosion Science* **2017**, *120*, 239–250.

[35] Y. Xiang, C. Li, Z. Long, C. Guan, W. Wang, W. Hesitao, *Electrochimica Acta* **2017**, *258*, 909–918.
[36] O. Barcia, O. R. Mattos, *Electrochimica Acta* **1990**, *35 (10)* 1601-1608.

[37] F. Farelas, M. Galicia, B. Brown, S. Nesic, H. Castaneda, *Corrosion Science* **2010**, *52*, 509–517.
[38] B. Kinsella, Y. J. Tan, and S. Bailey, *CORROSION* **1998**, *54*, 835–842.
[39] F. Pessu, R. Barker, A. Neville, *CORROSION* **2016**, 72 (1) 78-94.
[40] F. Pessu, PhD thesis, Leeds University, **2015**.
[41] M. B. Kermani and A. Morshed *Corrosion,* **2003,** 59 (8) 659–683.
[42] G. R. Joshi, K. Cooper, X. Zhong, A. B. Cook, E. A. Ahmad, N. M. Harrison, D. L. Engelberg, R. Lindsay, *Corrosion Science* **2018**, *142*, 110–118.
[43] J. B. Han, D. Young, H. Colijn, A. Tripathi, S. Nesic, *Industrial & Engineering Chemistry Research* **2009**, *48*, U191-U194.
[44] R. A. de Motte, *PhD thesis*, University of Leeds, **2016**.
[45] S. Nesic, M. Nordsveen, R. Nyborg, A. Stangeland, *CORROSION* **2003**, *59*, 489–497.
[46] M. L. Johnson, M. B. Tomson in *Corrosion 91/268*, **1991**.
[47] W. Li, B. Brown, D. Young, S. Nesic, *CORROSION* **2014**, *70*, 294–302.
[48] W. Li, MSc Thesis, Ohio University **2011**.
[49] a) R. de Motte, E. Basilico, R. Mingant, J. Kittel, F. Ropital, P. Combrade, S. Necib, V. Deydier, D. Crusset, S. Marcelin, *Corrosion Science 172 108666 ,* **2020**, b) G. A. Zhang, M. X. Lu, Y. B. Qiu, X. P. Guo, Z. Y. Chen, *J. Electrochem. Soc.* **2012**, *159*, C393-C402;
[50] a) M. Stern, A. L. Geaby, *J. Electrochem. Soc.* **1957**, *104*, 56; b) M. Stern, E.D. Weisert, *Proc. Am. Soc. Test. Mater.* **1959**, *59*, 1280;
[51] Q. Y. Liu, L. J. Mao, S. W. Zhou, *Corrosion Science* **2014**, *84*, 165–171.
[52] B. Ingham, M. Ko, N. Laycock, J. Burnell, P. Kappen, J. A. Kimpton, D. E. Williams, *Corrosion Science* **2012**, *56*, 96–104.
[53] S. Papavinasam, A. Doiron, and R. W. Revie, *Corrosion Science* **2009**, 65.10 (2009): 663-673.
[54] H. Fang, B. Brown, S. Nešić, *CORROSION* **2013**, *69*, 297–302.
[55] J. B. Han, J. W. Carey, J. S. Zhang, *Journal of Applied Electrochemistry* **2011**, *41*, 741–749.
[56] F. F. Eliyan, F. Mohammadi, A. Alfantazi, *Corrosion Science* **2012**, *64*, 37–43.
[57] S. Zhang, L. Hou, H. Du, H. Wei, B. Liu, Y. Wei, *Corrosion Science* **2020**, *167*, 108531.
[58] S. Zhang, L. Hou, H. Du, H. Wei, B. Liu, Y. Wei, *Vacuum* **2019**, *167*, 389–392.
[59] S. N. Esmaeely, Y.-S. Choi, D. Young, S. Nesic, *Materials Performance* **2014**, *53*, 54–59.
[60] A. G. Collins, Ed, *Developments in Petroleum Science : Geochemistry of Oilfield Waters*: Chapter 7. Origin of Oilfield Waters, Elsevier, **1975**.
[61] H.A. Alsaiari, MSc Thesis Rice university, **2008** .
[62] H. A. Alsaiari, A. T. Kan, M. B. Tomson in SPE International Conference on Oilfield Scale SPE-121553-MS, **2009**.
[63] H. A. Alsaiari, N. Zhang, S. Work, A. T. Kan, M. B. Tomson in SPE International Conference on Oilfield Scale, SPE-155127-MS, **2012**.
[64] S. Navabzadeh Esmaeely, Y.-S. Choi, D. Young, S. Nešić, *CORROSION* **2013**, *69*, 912–920.
[65] C. Ding, K. Gao, C. Chen, *International Journal of Minerals, Metallurgy and Materials* **2009**, *16*, 661–666.
[66] S. N. Esmaeely, D. Young, B. Brown, S. Nešić, *CORROSION* **2016**, *73*, 238–246.
[67] Z. D. Cui, S. L. Wu, S. L. Zhu, X. J. Yang, *Applied Surface Science* **2006**, *252*, 2368–2374.
[68] S. L. Wu, Z. D. Cui, F. He, Z. Q. Bai, S. L. Zhu, X. J. Yang, *Materials Letters* **2004**, *58*, 1076–1081.

[69] L. M. Tavares, E. M. d. Costa, J. J. d. O. Andrade, R. Hubler, B. Huet, *Applied Surface Science* **2015**, *359*, 143–152.
[70] A. Shamsa, R. Barker, Y. Hua, E. Barmatov, T. L. Hughes, A. Neville, *Corrosion Science* **2019**, *156*, 58–70.
[71] Y. Xiang, Z. Wang, X. Yang, Z. Li, W. Ni, *The Journal of Supercritical Fluids* **2012**, *67*, 14–21.
[72] J. Sun, C. Sun, G. Zhang, X. Li, W. Zhao, T. Jiang, H. Liu, X. Cheng, Y. Wang, *Corrosion Science* **2016**, *107*, 31–40.
[73] S. Wang, MSc thesis Ohio University, **2009**.
[74] Nor Roslina Rosli, PhD thesis Ohio University, **2015**.
[75] B. Ingham, M. Ko, P. Shaw, Mobbassar Hassan Sk, Aboubakar M. Abdullah, N. Laycock, D.E. Williams, *Journal of the Electrochemical Society* **2018**, *165(11) C756-C761*.
[76] B. Ingham, M. Ko, N. Laycock, N. M. Kirby, D. E. Williams, *Faraday discussions* **2015**, *180*, 171–190.
[77] I. Azoulay, C. Rémazeilles, P. Refait, *Corrosion Science* **2014**, *85*, 101–108.

Competing interests
The authors declare that they have no competing interests

Funding
IFP Energies Nouvelles financed this research.

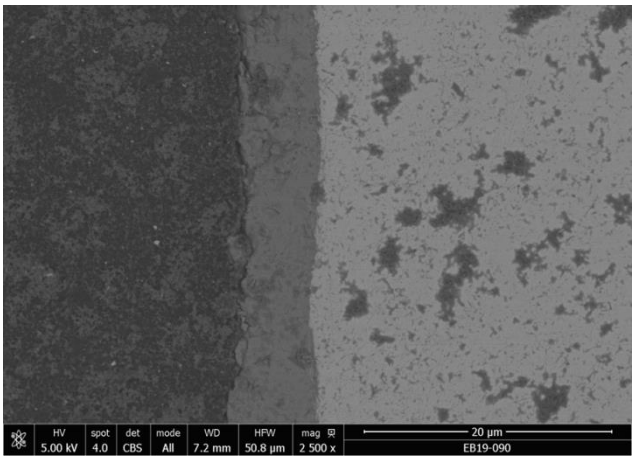

Figure 1 Cross section SEM micrograph of the corrosion product layer of a CO2 saturate water solutionat 80°C pH 6.8.

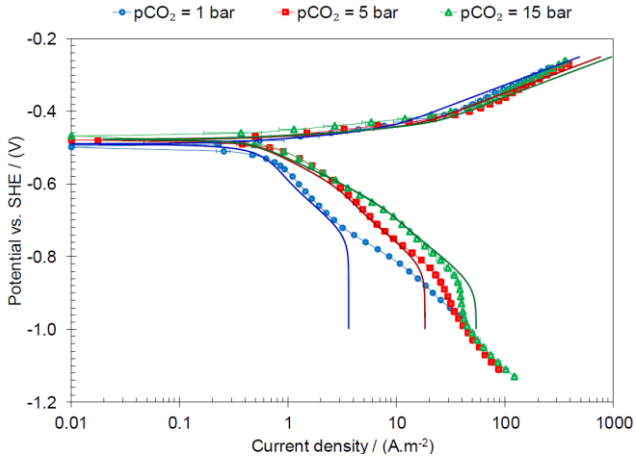

Figure 2 Polarizations curves on API 5L X65 mild steel at 10°C, 0.1 M NaCl, 4.4 m/s flow velocity, at pCO2 of 1, 5, and 15 bar, at pH 6. Solid lines represent modeling with “buffer mechanism” [21].

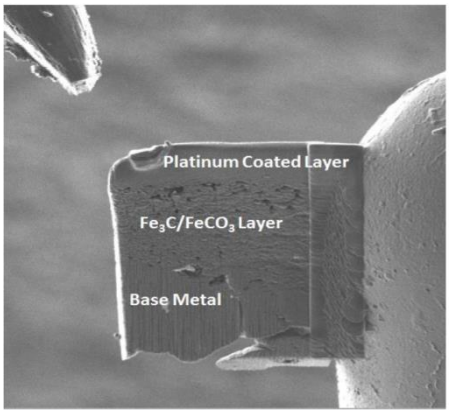

Figure 3 cross section TEM image of a of corrosion product on X65 steel on a CO2 saturated 10 wt% NaCl at 80°C after 168 h [43].

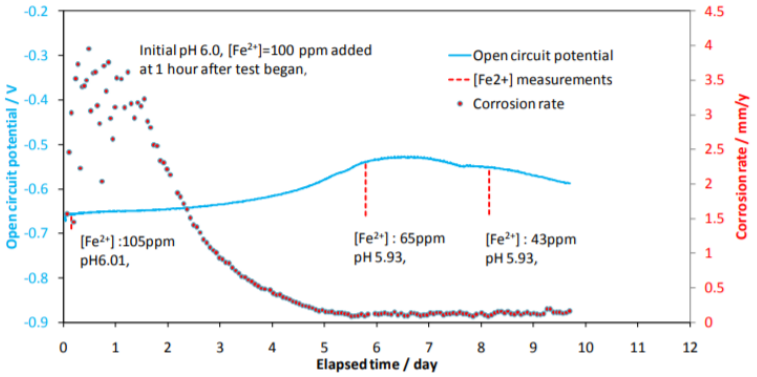

Figure 4 OCP variations and corrosion rate as function of exposure time at 80°C, pH 6.0, 0.53 bar 53 kPa CO2, 1 wt% NaCl [51].

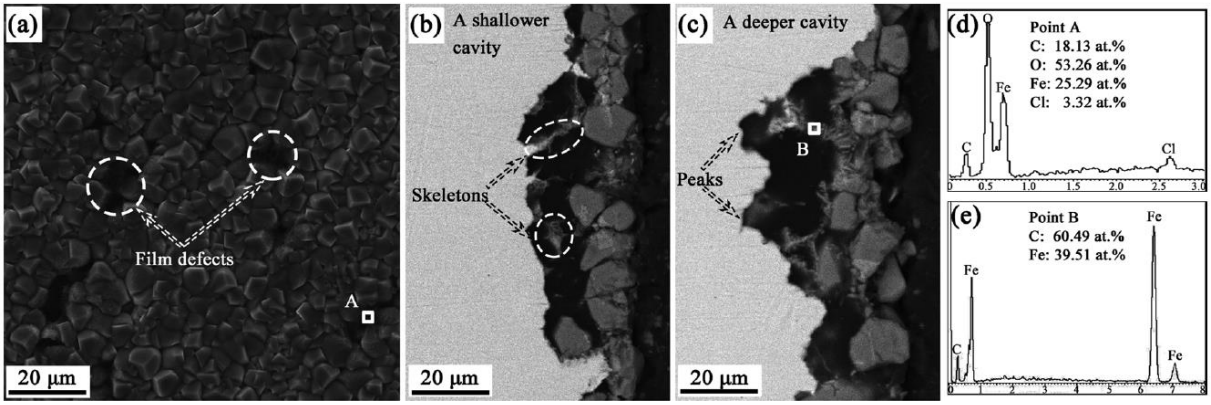

Figure 5 SEM micrographs (a) − (c) of morphologies of corrosion product layer for carbon steel in Cl-containing CO2 saturated solution. (d) −(e) relative EDS analysis [62].

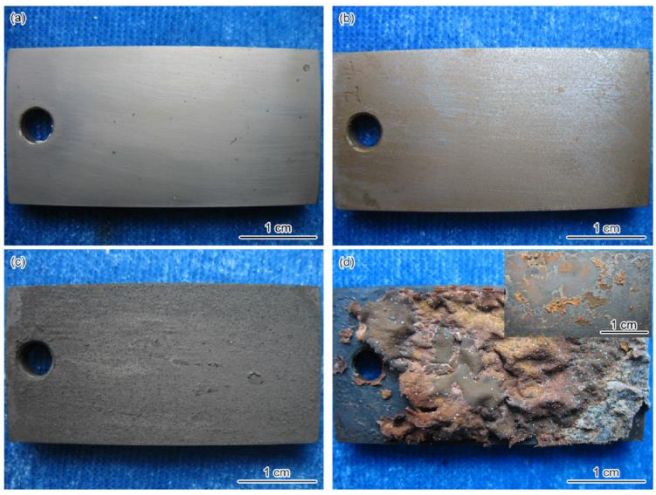

Figure 6 Photograps of corrosion product layer developed at 50°C CO2, 10 MPa, O2: 2000 ppmv, H2S: 2000 ppmv. (a) CO2; (b) CO2+ O2; (c) CO2+ H2S and (d) CO2+ O2+ H2S [77].